

High-Speed Tracking with Kernelized Correlation Filters

João F. Henriques, Rui Caseiro, Pedro Martins, and Jorge Batista

Abstract—The core component of most modern trackers is a discriminative classifier, tasked with distinguishing between the target and the surrounding environment. To cope with natural image changes, this classifier is typically trained with translated and scaled sample patches. Such sets of samples are riddled with redundancies—any overlapping pixels are constrained to be the same. Based on this simple observation, we propose an analytic model for datasets of thousands of translated patches. By showing that the resulting data matrix is circulant, we can diagonalize it with the discrete Fourier transform, reducing both storage and computation by several orders of magnitude. Interestingly, for linear regression our formulation is equivalent to a correlation filter, used by some of the fastest competitive trackers. For kernel regression, however, we derive a new kernelized correlation filter (KCF), that unlike other kernel algorithms has the exact same complexity as its linear counterpart. Building on it, we also propose a fast multi-channel extension of linear correlation filters, via a linear kernel, which we call dual correlation filter (DCF). Both KCF and DCF outperform top-ranking trackers such as Struck or TLD on a 50 videos benchmark, despite running at hundreds of frames-per-second, and being implemented in a few lines of code (Algorithm 1). To encourage further developments, our tracking framework was made open-source.



Index Terms—Visual tracking, circulant matrices, discrete Fourier transform, kernel methods, ridge regression, correlation filters



1 INTRODUCTION

ARGUABLY one of the biggest breakthroughs in recent visual tracking research was the widespread adoption of discriminative learning methods. The task of tracking, a crucial component of many computer vision systems, can be naturally specified as an online learning problem [1], [2]. Given an initial image patch containing the target, the goal is to learn a classifier to discriminate between its appearance and that of the environment. This classifier can be evaluated exhaustively at many locations, in order to detect it in subsequent frames. Of course, each new detection provides a new image patch that can be used to update the model.

It is tempting to focus on characterizing the object of interest—the positive samples for the classifier. However, a core tenet of discriminative methods is to give as much importance, or more, to the relevant environment—the negative samples. The most commonly used negative samples are image patches from different locations and scales, reflecting the prior knowledge that the classifier will be evaluated under those conditions.

An extremely challenging factor is the virtually unlimited amount of negative samples that can be obtained from an image. Due to the time-sensitive nature of tracking, modern trackers walk a fine line between incorporating as many samples as possible and keeping computational demand low. It is common practice to randomly choose only a few samples each frame [3], [4], [5], [6], [7].

• The authors are with the Institute of Systems and Robotics, University of Coimbra, Coimbra, Portugal.

E-mail: {henriques, ruicaseiro, pedromartins, batista}@isr.uc.pt

Manuscript received 17 Mar. 2014; revised 11 July 2014; accepted 28 July 2014. Date of publication 31 July 2014; date of current version 13 Feb. 2015.

Recommended for acceptance by E. G. Learned-Miller.

For information on obtaining reprints of this article, please send e-mail to: reprints@ieee.org, and reference the Digital Object Identifier below.

Digital Object Identifier no. 10.1109/TPAMI.2014.2345390

Although the reasons for doing so are understandable, we argue that undersampling negatives is the main factor inhibiting performance in tracking. In this paper, we develop tools to analytically incorporate thousands of samples at different relative translations, without iterating over them explicitly. This is made possible by the discovery that, in the Fourier domain, some learning algorithms actually become easier as we add more samples, if we use a specific model for translations.

These analytical tools, namely circulant matrices, provide a useful bridge between popular learning algorithms and classical signal processing. The implication is that we are able to propose a tracker based on kernel ridge regression [8] that does not suffer from the “curse of kernelization”, which is its larger asymptotic complexity, and even exhibits lower complexity than unstructured linear regression. Instead, it can be seen as a kernelized version of a linear correlation filter, which forms the basis for the fastest trackers available [9], [10]. We leverage the powerful kernel trick at the same computational complexity as linear correlation filters. Our framework easily incorporates multiple feature channels, and by using a linear kernel we show a fast extension of linear correlation filters to the multi-channel case.



2 RELATED WORK

2.1 On Tracking-by-Detection

A comprehensive review of tracking-by-detection is outside the scope of this article, but we refer the interested reader to two excellent and very recent surveys [1], [2]. The most popular approach is to use a discriminative appearance model [3], [4], [5], [6]. It consists of training a classifier online, inspired by statistical machine learning methods, to predict the presence or absence of the target in an image patch. This classifier is then tested on many candidate patches to find the most likely location.

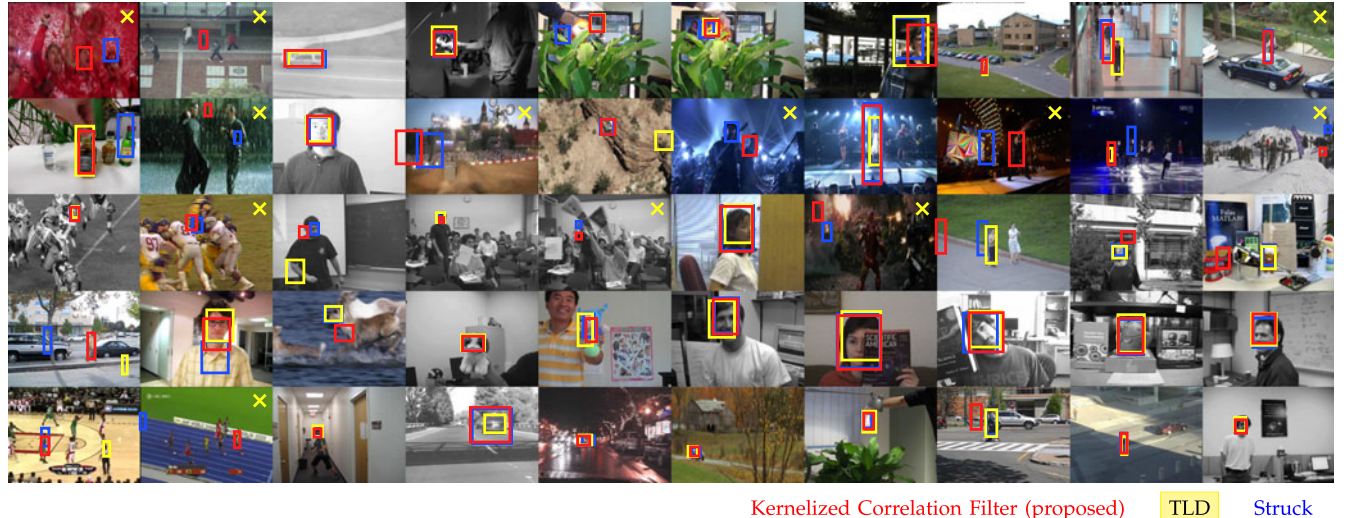


Fig. 1. Qualitative results for the proposed KCF, compared with the top-performing Struck and TLD. Best viewed on a high-resolution screen. The chosen kernel is Gaussian, on HOG features. These snapshots were taken at the midpoints of the 50 videos of a recent benchmark [11]. Missing trackers are denoted by an “x”. KCF outperforms both Struck and TLD, despite its minimal implementation and running at 172 FPS (see Algorithm 1, and Table 1).

Alternatively, the position can also be predicted directly [7]. Regression with class labels can be seen as classification, so we use the two terms interchangeably.

We will discuss some relevant trackers before focusing on the literature that is more directly related to our analytical methods. Canonical examples of the tracking-by-detection paradigm include those based on support vector machines (SVM) [12], random forest classifiers [6], or boosting variants [5], [13]. All the mentioned algorithms had to be adapted for online learning, in order to be useful for tracking. Zhang et al. [3] propose a projection to a fixed random basis, to train a Naive Bayes classifier, inspired by compressive sensing techniques. Aiming to predict the target’s location directly, instead of its presence in a given image patch, Hare et al. [7] employed a structured output SVM and Gaussian kernels, based on a large number of image features. Examples of non-discriminative trackers include the work of Wu et al. [14], who formulate tracking as a sequence of image alignment objectives, and of Sevilla-Lara and Learned-Miller [15], who propose a strong appearance descriptor based on distribution fields. Another discriminative approach by Kalal et al. [4] uses a set of structural constraints to guide the sampling process of a boosting classifier. Finally, Bolme et al. [9] employ classical signal processing analysis to derive fast correlation filters. We will discuss these last two works in more detail shortly.

2.2 On Sample Translations and Correlation Filtering

Recall that our goal is to learn and detect over translated image patches efficiently. Unlike our approach, most attempts so far have focused on trying to weed out irrelevant image patches. On the detection side, it is possible to use branch-and-bound to find the maximum of a classifier’s response while avoiding unpromising candidate patches [16]. Unfortunately, in the worst-case the algorithm may still have to iterate over all patches. A related method finds the most similar patches of a pair of images efficiently [17], but is not directly translated to our setting. Though it does

not preclude an exhaustive search, a notable optimization is to use a fast but inaccurate classifier to select promising patches, and only apply the full, slower classifier on those [18], [19].

On the training side, Kalal et al. [4] propose using structural constraints to select relevant sample patches from each new image. This approach is relatively expensive, limiting the features that can be used, and requires careful tuning of the structural heuristics. A popular and related method, though it is mainly used in offline detector learning, is hard-negative mining [20]. It consists of running an initial detector on a pool of images, and selecting any wrong detections as samples for re-training. Even though both approaches reduce the number of training samples, a major drawback is that the candidate patches have to be considered exhaustively, by running a detector.

The initial motivation for our line of research was the recent success of correlation filters in tracking [9], [10]. Correlation filters have proved to be competitive with far more complicated approaches, but using only a fraction of the computational power, at hundreds of frames-per-second. They take advantage of the fact that the convolution of two patches (loosely, their dot-product at different relative translations) is equivalent to an element-wise product in the Fourier domain. Thus, by formulating their objective in the Fourier domain, they can specify the desired output of a linear classifier for several translations, or image shifts, at once.

A Fourier domain approach can be very efficient, and has several decades of research in signal processing to draw from [21]. Unfortunately, it can also be extremely limiting. We would like to simultaneously leverage more recent advances in computer vision, such as more powerful features, large-margin classifiers or kernel methods [20], [22], [23].

A few studies go in that direction, and attempt to apply kernel methods to correlation filters [24], [25], [26], [27]. In these works, a distinction must be drawn between two types of objective functions: those that do not consider the power spectrum or image translations, such as synthetic

discriminant function (SDF) filters [25], [26], and those that do, such as minimum average correlation energy [28], optimal trade-off [27] and minimum output sum of squared error (MOSSE) filters [9]. Since the spatial structure can effectively be ignored, the former are easier to kernelize, and Kernel SDF filters have been proposed [25], [26], [27]. However, lacking a clearer relationship between translated images, non-linear kernels and the Fourier domain, applying the kernel trick to other filters has proven much more difficult [24], [25], with some proposals requiring significantly higher computation times and imposing strong limits on the number of image shifts that can be considered [24].

For us, this hinted that a deeper connection between translated image patches and training algorithms was needed, in order to overcome the limitations of direct Fourier domain formulations.

2.3 Subsequent Work

Since the initial version of this work [29], an interesting time-domain variant of the proposed cyclic shift model has been used very successfully for video event retrieval [30]. Generalizations of linear correlation filters to multiple channels have also been proposed [31], [32], [33], some of which building on our initial work. This allows them to leverage more modern features (e.g. Histogram of Oriented Gradients—HOG). A generalization to other linear algorithms, such as support vector regression, was also proposed [31]. We must point out that all of these works target off-line training, and thus rely on slower solvers [31], [32], [33]. In contrast, we focus on fast element-wise operations, which are more suitable for real-time tracking, even with the kernel trick.

3 CONTRIBUTIONS

A preliminary version of this work was presented earlier [29]. It demonstrated, for the first time, the connection between ridge regression with cyclically shifted samples and classical correlation filters. This enabled fast learning with $\mathcal{O}(n \log n)$ fast Fourier transforms instead of expensive matrix algebra. The first kernelized correlation filter was also proposed, though limited to a single channel. Additionally, it proposed closed-form solutions to compute kernels at all cyclic shifts. These carried the same $\mathcal{O}(n \log n)$ computational cost, and were derived for radial basis and dot-product kernels.

The present work adds to the initial version in significant ways. All the original results were re-derived using a much simpler diagonalization technique (Sections 4, 5, and 6). We extend the original work to deal with multiple channels, which allows the use of state-of-the-art features that give an important boost to performance (Section 7). Considerable new analysis and intuitive explanations are added to the initial results. We also extend the original experiments from 12 to 50 videos, and add a new variant of the Kernelized Correlation Filter (KCF) tracker based on Histogram of Oriented Gradients (HOG) features instead of raw pixels. Via a linear kernel, we additionally propose a linear multi-channel filter with very low computational complexity, that almost matches the performance of non-linear kernels. We name it Dual Correlation Filter (DCF), and show how it is related to

a set of recent, more expensive multi-channel filters [31]. Experimentally, we demonstrate that the KCF already performs better than a linear filter, without any feature extraction. With HOG features, both the linear DCF and non-linear KCF outperform by a large margin top-ranking trackers, such as Struck [7] or Track-Learn-Detect (TLD) [4], while comfortably running at hundreds of frames-per-second.

4 BUILDING BLOCKS

In this section, we propose an analytical model for image patches extracted at different translations, and work out the impact on a linear regression algorithm. We will show a natural underlying connection to classical correlation filters. The tools we develop will allow us to study more complicated algorithms in Sections 5, 6, and 7.

4.1 Linear Regression

We will focus on ridge regression, since it admits a simple closed-form solution, and can achieve performance that is close to more sophisticated methods, such as Support Vector Machines [8]. The goal of training is to find a function $f(\mathbf{z}) = \mathbf{w}^T \mathbf{z}$ that minimizes the squared error over samples \mathbf{x}_i and their regression targets y_i ,

$$\min_{\mathbf{w}} \sum_i (f(\mathbf{x}_i) - y_i)^2 + \lambda \|\mathbf{w}\|^2. \quad (1)$$

The λ is a regularization parameter that controls overfitting, as in the SVM. As mentioned earlier, the minimizer has a closed-form, which is given by [8]

$$\mathbf{w} = (X^T X + \lambda I)^{-1} X^T \mathbf{y}, \quad (2)$$

where the data matrix X has one sample per row \mathbf{x}_i , and each element of \mathbf{y} is a regression target y_i . I is an identity matrix.

Starting in Section 4.4, we will have to work in the Fourier domain, where quantities are usually complex-valued. They are not harder to deal with, as long as we use the complex version of Eq. (2) instead,

$$\mathbf{w} = (X^H X + \lambda I)^{-1} X^H \mathbf{y}, \quad (3)$$

where X^H is the Hermitian transpose, i.e., $X^H = (X^*)^T$, and X^* is the complex-conjugate of X . For real numbers, Eq. (3) reduces to Eq. (2).

In general, a large system of linear equations must be solved to compute the solution, which can become prohibitive in a real-time setting. Over the next paragraphs we will see a special case of \mathbf{x}_i that bypasses this limitation.

4.2 Cyclic Shifts

For notational simplicity, we will focus on single-channel, one-dimensional signals. These results generalize to multi-channel, two-dimensional images in a straightforward way (Section 7).

Consider an $n \times 1$ vector representing a patch with the object of interest, denoted \mathbf{x} . We will refer to it as the *base sample*. Our goal is to train a classifier with both the base sample (a positive example) and several virtual samples obtained by translating it (which serve as negative examples). We can

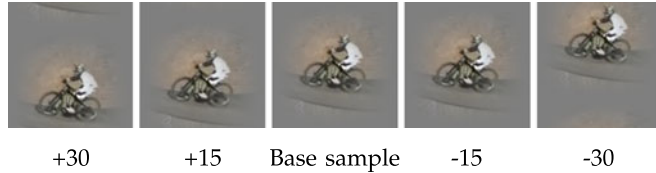


Fig. 2. Examples of vertical cyclic shifts of a base sample. Our Fourier domain formulation allows us to train a tracker with *all* possible cyclic shifts of a base sample, both vertical and horizontal, without iterating them explicitly. Artifacts from the wrapped-around edges can be seen (top of the left-most image), but are mitigated by the cosine window and padding.

model one-dimensional translations of this vector by a *cyclic shift operator*, which is the permutation matrix

$$P = \begin{bmatrix} 0 & 0 & 0 & \cdots & 1 \\ 1 & 0 & 0 & \cdots & 0 \\ 0 & 1 & 0 & \cdots & 0 \\ \vdots & \vdots & \ddots & \ddots & \vdots \\ 0 & 0 & \cdots & 1 & 0 \end{bmatrix}. \quad (4)$$

The product $P\mathbf{x} = [x_n, x_1, x_2, \dots, x_{n-1}]^T$ shifts \mathbf{x} by one element, modeling a small translation. We can chain u shifts to achieve a larger translation by using the matrix power $P^u\mathbf{x}$. A negative u will shift in the reverse direction. A 1D signal translated horizontally with this model is illustrated in Fig. 3, and an example for a 2D image is shown in Fig. 2.

The attentive reader will notice that the last element wraps around, inducing some distortion relative to a true translation. However, this undesirable property can be mitigated by appropriate padding and windowing (Appendix A.1). The fact that a large percentage of the elements of a signal are still modeled correctly, even for relatively large translations (see Fig. 2), explains the observation that cyclic shifts work well in practice.

Due to the cyclic property, we get the same signal \mathbf{x} periodically every n shifts. This means that the full set of shifted signals is obtained with

$$\{P^u\mathbf{x} \mid u = 0, \dots, n-1\}. \quad (5)$$

Again due to the cyclic property, we can equivalently view the first half of this set as shifts in the positive direction, and the second half as shifts in the negative direction.

4.3 Circulant Matrices

To compute a regression with shifted samples, we can use the set of Eq. (5) as the rows of a data matrix X :

$$X = C(\mathbf{x}) = \begin{bmatrix} x_1 & x_2 & x_3 & \cdots & x_n \\ x_n & x_1 & x_2 & \cdots & x_{n-1} \\ x_{n-1} & x_n & x_1 & \cdots & x_{n-2} \\ \vdots & \vdots & \vdots & \ddots & \vdots \\ x_2 & x_3 & x_4 & \cdots & x_1 \end{bmatrix}. \quad (6)$$

An illustration of the resulting pattern is given in Fig. 3. What we have just arrived at is a *circulant matrix*, which has several intriguing properties [34], [35]. Notice that the pattern is deterministic, and fully specified by the generating vector \mathbf{x} , which is the first row.

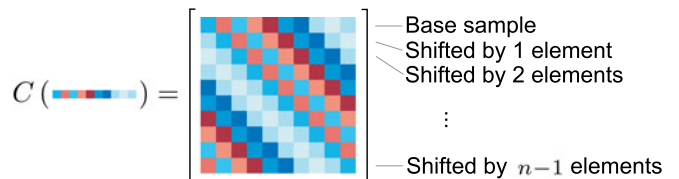


Fig. 3. Illustration of a circulant matrix. The rows are cyclic shifts of a vector image, or its translations in 1D. The same properties carry over to circulant matrices containing 2D images.

What is perhaps most amazing and useful is the fact that **all circulant matrices are made diagonal by the discrete Fourier transform (DFT), regardless of the generating vector \mathbf{x}** [34]. This can be expressed as

$$X = F \text{diag}(\hat{\mathbf{x}}) F^H, \quad (7)$$

where F is a constant matrix that does not depend on \mathbf{x} , and $\hat{\mathbf{x}}$ denotes the DFT of the generating vector, $\hat{\mathbf{x}} = \mathcal{F}(\mathbf{x})$. From now on, we will always use a hat $\hat{\cdot}$ as shorthand for the DFT of a vector.

The constant matrix F is known as the *DFT matrix*, and is the unique matrix that computes the DFT of any input vector, as $\mathcal{F}(\mathbf{z}) = \sqrt{n}F\mathbf{z}$. This is possible because the DFT is a linear operation.

Eq. (7) expresses the eigendecomposition of a general circulant matrix. The shared, deterministic eigenvectors F lie at the root of many uncommon features, such as commutativity or closed-form inversion.

4.4 Putting It All Together

We can now apply this new knowledge to simplify the linear regression in Eq. (3), when the training data is composed of cyclic shifts. Being able to work solely with diagonal matrices is very appealing, because all operations can be done element-wise on their diagonal elements.

Take the term $X^H X$, which can be seen as a non-centered covariance matrix. Replacing Eq. (7) in it,

$$X^H X = F \text{diag}(\hat{\mathbf{x}}^*) F^H F \text{diag}(\hat{\mathbf{x}}) F^H. \quad (8)$$

Since diagonal matrices are symmetric, taking the Hermitian transpose only left behind a complex-conjugate, $\hat{\mathbf{x}}^*$. Additionally, we can eliminate the factor $F^H F = I$. This property is the unitarity of F and can be canceled out in many expressions. We are left with

$$X^H X = F \text{diag}(\hat{\mathbf{x}}^*) \text{diag}(\hat{\mathbf{x}}) F^H. \quad (9)$$

Because operations on diagonal matrices are element-wise, we can define the element-wise product as \odot and obtain

$$X^H X = F \text{diag}(\hat{\mathbf{x}}^* \odot \hat{\mathbf{x}}) F^H. \quad (10)$$

An interesting aspect is that the vector in brackets is known as the *auto-correlation* of the signal \mathbf{x} (in the Fourier domain, also known as the *power spectrum* [21]). In classical signal processing, it contains the variance of a time-varying process for different time lags, or in our case, space.

The above steps summarize the general approach taken in diagonalizing expressions with circulant matrices.

Applying them recursively to the full expression for linear regression (Eq. (3)), we can put most quantities inside the diagonal,

$$\hat{\mathbf{w}} = \text{diag}\left(\frac{\hat{\mathbf{x}}^*}{\hat{\mathbf{x}}^* \odot \hat{\mathbf{x}} + \lambda}\right)\hat{\mathbf{y}}, \quad (11)$$

or better yet,

$$\hat{\mathbf{w}} = \frac{\hat{\mathbf{x}}^* \odot \hat{\mathbf{y}}}{\hat{\mathbf{x}}^* \odot \hat{\mathbf{x}} + \lambda}. \quad (12)$$

这个相除是点除运算，即对应元素相除

The fraction denotes element-wise division. We can easily recover \mathbf{w} in the spatial domain with the Inverse DFT, which has the same cost as a forward DFT. The detailed steps of the recursive diagonalization that yields Eq. (12) are given in Appendix A.5.

At this point we just found an unexpected formula from classical signal processing—the solution is a regularized correlation filter [9], [21].

Before exploring this relation further, we must highlight the computational efficiency of Eq. (12), compared to the prevalent method of extracting patches explicitly and solving a general regression problem. For example, ridge regression has a cost of $\mathcal{O}(n^3)$, bound by the matrix inversion and products.¹ On the other hand, all operations in Eq. (12) are element-wise ($\mathcal{O}(n)$), except for the DFT, which bounds the cost at a nearly-linear $\mathcal{O}(n \log n)$. For typical data sizes, this reduces storage and computation by several orders of magnitude.

4.5 Relationship to Correlation Filters

Correlation filters have been a part of signal processing since the 80's, with solutions to a myriad of objective functions in the Fourier domain [21], [28]. Recently, they made a reappearance as MOSSE filters [9], which have shown remarkable performance in tracking, despite their simplicity and high FPS rate.

The solution to these filters looks like Eq. (12) (see Appendix A.2), but with two crucial differences. First, MOSSE filters are derived from an objective function specifically formulated in the Fourier domain. Second, the λ regularizer is added in an ad-hoc way, to avoid division-by-zero. The derivation we showed above adds considerable insight, by specifying the starting point as ridge regression with cyclic shifts, and arriving at the same solution.

Circulant matrices allow us to enrich the toolset put forward by classical signal processing and modern correlation filters, and apply the Fourier trick to new algorithms. Over the next section we will see one such instance, in training non-linear filters.

5 NON-LINEAR REGRESSION

One way to allow more powerful, non-linear regression functions $f(\mathbf{z})$ is with the “kernel trick” [23]. The most

1. We remark that the complexity of training algorithms is usually reported in terms of the number of samples n , disregarding the number of features m . Since in our case $m = n$ (X is square), we conflate the two quantities. For comparison, the fastest SVM solvers have “linear” complexity in the samples $\mathcal{O}(mn)$, but under the same conditions $m = n$ would actually exhibit quadratic complexity, $\mathcal{O}(n^2)$.

attractive quality is that the optimization problem is still linear, albeit in a different set of variables (the *dual space*). On the downside, evaluating $f(\mathbf{z})$ typically grows in complexity with the number of samples.

Using our new analysis tools, however, we will show that it is possible to overcome this limitation, and obtain non-linear filters that are *as fast as linear correlation filters*, both to train and evaluate.

5.1 Kernel Trick – Brief Overview

This section will briefly review the kernel trick, and define the relevant notation.

Mapping the inputs of a linear problem to a non-linear feature-space $\varphi(\mathbf{x})$ with the kernel trick consists of:

- 1) Expressing the solution \mathbf{w} as a linear combination of the samples:

$$\mathbf{w} = \sum_i \alpha_i \varphi(\mathbf{x}_i). \quad (13)$$

The variables under optimization are thus α , instead of \mathbf{w} . This alternative representation α is said to be in the *dual space*, as opposed to the *primal space* \mathbf{w} (Representer Theorem [23, p. 89]).

- 2) Writing the algorithm in terms of dot-products $\varphi^T(\mathbf{x})\varphi(\mathbf{x}') = \kappa(\mathbf{x}, \mathbf{x}')$, which are computed using the kernel function κ (e.g., Gaussian or Polynomial).

The dot-products between all pairs of samples are usually stored in a $n \times n$ kernel matrix K , with elements

$$K_{ij} = \kappa(\mathbf{x}_i, \mathbf{x}_j). \quad (14)$$

The power of the kernel trick comes from the implicit use of a high-dimensional feature space $\varphi(\mathbf{x})$, without ever instantiating a vector in that space. Unfortunately, this is also its greatest weakness, since the regression function’s complexity grows with the number of samples,

$$f(\mathbf{z}) = \mathbf{w}^T \mathbf{z} = \sum_{i=1}^n \alpha_i \kappa(\mathbf{z}, \mathbf{x}_i). \quad (15)$$

In the coming sections we will show how most drawbacks of the kernel trick can be avoided, assuming circulant data.

5.2 Fast Kernel Regression

The solution to the kernelized version of ridge regression is given by [8]

$$\alpha = (K + \lambda I)^{-1} \mathbf{y}, \quad (16)$$

where K is the kernel matrix and α is the vector of coefficients α_i , that represent the solution in the dual space.

Now, if we can prove that K is circulant for datasets of cyclic shifts, we can diagonalize Eq. (16) and obtain a fast solution as for the linear case. This would seem to be intuitively true, but does not hold in general. The arbitrary non-linear mapping $\varphi(\mathbf{x})$ gives us no guarantee of preserving any sort of structure. However, we can impose one condition that will allow K to be circulant. It turns out to be fairly broad, and apply to most useful kernels.

Theorem 1. Given circulant data $C(\mathbf{x})$, the corresponding kernel matrix K is circulant if the kernel function satisfies $\kappa(\mathbf{x}, \mathbf{x}') = \kappa(M\mathbf{x}, M\mathbf{x}')$, for any permutation matrix M .

For a proof, see Appendix A.2. What this means is that, for a kernel to preserve the circulant structure, it must treat all dimensions of the data equally. Fortunately, this includes most useful kernels. 

Example 2. The following kernels satisfy Theorem 1:

- Radial Basis Function kernels—e.g., Gaussian.
- Dot-product kernels—e.g., linear, polynomial.
- Additive kernels—e.g., intersection, χ^2 and Hellinger kernels [36].
- Exponentiated additive kernels. 

Checking this fact is easy, since reordering the dimensions of \mathbf{x} and \mathbf{x}' simultaneously does not change $\kappa(\mathbf{x}, \mathbf{x}')$ for these kernels. This applies to any kernel that combines dimensions through a commutative operation, such as sum, product, min and max.

Knowing which kernels we can use to make K circulant, it is possible to diagonalize Eq. (16) as in the linear case, obtaining

$$\hat{\alpha} = \frac{\hat{\mathbf{y}}}{\hat{\mathbf{k}}^{\mathbf{x}\mathbf{x}} + \lambda}, \quad (17)$$

where $\hat{\mathbf{k}}^{\mathbf{x}\mathbf{x}}$ is the first row of the kernel matrix $K = C(\mathbf{k}^{\mathbf{x}\mathbf{x}})$, and again a hat ^ denotes the DFT of a vector. A detailed derivation is in Appendix A.3. 

To better understand the role of $\hat{\mathbf{k}}^{\mathbf{x}\mathbf{x}}$, we found it useful to define a more general *kernel correlation*. The kernel correlation of two arbitrary vectors, \mathbf{x} and \mathbf{x}' , is the vector $\mathbf{k}^{\mathbf{x}\mathbf{x}'}$ with elements

$$k_i^{\mathbf{x}\mathbf{x}'} = \kappa(\mathbf{x}', P^{i-1}\mathbf{x}). \quad (18)$$

In words, it contains the kernel evaluated for different relative shifts of the two arguments. Then $\hat{\mathbf{k}}^{\mathbf{x}\mathbf{x}}$ is the kernel correlation of \mathbf{x} with itself, in the Fourier domain. We can refer to it as the *kernel auto-correlation*, in analogy with the linear case. 

This analogy can be taken further. Since a kernel is equivalent to a dot-product in a high-dimensional space $\varphi(\cdot)$, another way to view Eq. (18) is

$$k_i^{\mathbf{x}\mathbf{x}'} = \varphi^T(\mathbf{x}')\varphi(P^{i-1}\mathbf{x}), \quad (19)$$

which is the cross-correlation of \mathbf{x} and \mathbf{x}' in the high-dimensional space $\varphi(\cdot)$. 

Notice how we only need to compute and operate on the kernel auto-correlation, an $n \times 1$ vector, which grows linearly with the number of samples. This is contrary to the conventional wisdom on kernel methods, which requires computing an $n \times n$ kernel matrix, scaling quadratically with the samples. Our knowledge of the exact structure of K allowed us to do better than a generic algorithm. 

Finding the optimal α is not the only problem that can be accelerated, due to the ubiquity of translated patches in a tracking-by-detection setting. Over the next paragraphs we will investigate the effect of the cyclic shift model on the detection phase, and even in computing kernel correlations.

5.3 Fast Detection

It is rarely the case that we want to evaluate the regression function $f(\mathbf{z})$ for one image patch in isolation. To detect the object of interest, we typically wish to evaluate $f(\mathbf{z})$ on several image locations, i.e., for several candidate patches. These patches can be modeled by cyclic shifts. 

Denote by $K^{\mathbf{z}}$ the (asymmetric) kernel matrix between all training samples and all candidate patches. Since the samples and patches are cyclic shifts of base sample \mathbf{x} and base patch \mathbf{z} , respectively, each element of $K^{\mathbf{z}}$ is given by $\kappa(P^{i-1}\mathbf{z}, P^{j-1}\mathbf{x})$. It is easy to verify that this kernel matrix satisfies Theorem 1, and is circulant for appropriate kernels. 

Similarly to Section 5.2, we only need the first row to define the kernel matrix:

$$K^{\mathbf{z}} = C(\mathbf{k}^{\mathbf{x}\mathbf{z}}), \quad (20)$$

where $\mathbf{k}^{\mathbf{x}\mathbf{z}}$ is the *kernel correlation* of \mathbf{x} and \mathbf{z} , as defined before. 

From Eq. (15), we can compute the regression function for all candidate patches with

$$\mathbf{f}(\mathbf{z}) = (K^{\mathbf{z}})^T \boldsymbol{\alpha}. \quad (21)$$

Notice that $\mathbf{f}(\mathbf{z})$ is a vector, containing the output for all cyclic shifts of \mathbf{z} , i.e., the full detection response. To compute Eq. (21) efficiently, we diagonalize it to obtain 

$$\hat{\mathbf{f}}(\mathbf{z}) = \hat{\mathbf{k}}^{\mathbf{x}\mathbf{z}} \odot \hat{\boldsymbol{\alpha}}. \quad (22)$$

Intuitively, evaluating $f(\mathbf{z})$ at all locations can be seen as a spatial filtering operation over the kernel values $\mathbf{k}^{\mathbf{x}\mathbf{z}}$. Each $f(\mathbf{z})$ is a linear combination of the neighboring kernel values from $\mathbf{k}^{\mathbf{x}\mathbf{z}}$, weighted by the learned coefficients $\boldsymbol{\alpha}$. Since this is a filtering operation, it can be formulated more efficiently in the Fourier domain. 

6 FAST KERNEL CORRELATION

Even though we have found faster algorithms for training and detection, they still rely on computing one kernel correlation each ($\mathbf{k}^{\mathbf{x}\mathbf{x}}$ and $\mathbf{k}^{\mathbf{x}\mathbf{z}}$, respectively). Recall that kernel correlation consists of computing the kernel for all relative shifts of two input vectors. This represents the last standing computational bottleneck, as a naive evaluation of n kernels for signals of size n will have quadratic complexity. However, using the cyclic shift model will allow us to efficiently exploit the redundancies in this expensive computation. 

6.1 Dot-Product and Polynomial Kernels

Dot-product kernels have the form $\kappa(\mathbf{x}, \mathbf{x}') = g(\mathbf{x}^T \mathbf{x}')$, for some function g . Then, $\mathbf{k}^{\mathbf{x}\mathbf{x}'}$ has elements

$$k_i^{\mathbf{x}\mathbf{x}'} = \kappa(\mathbf{x}', P^{i-1}\mathbf{x}) = g(\mathbf{x}'^T P^{i-1}\mathbf{x}). \quad (23)$$

Let g also work element-wise on any input vector. This way we can write Eq. (23) in vector form

$$\mathbf{k}^{\mathbf{x}\mathbf{x}'} = g(C(\mathbf{x}) \mathbf{x}'). \quad (24)$$

This makes it an easy target for diagonalization, yielding

$$\mathbf{k}^{\mathbf{x}\mathbf{x}'} = g(\mathcal{F}^{-1}(\hat{\mathbf{x}}^* \odot \hat{\mathbf{x}}')), \quad (25)$$

where \mathcal{F}^{-1} denotes the inverse DFT.

In particular, for a polynomial kernel $\kappa(\mathbf{x}, \mathbf{x}') = (\mathbf{x}^T \mathbf{x}' + a)^b$,

$$\mathbf{k}^{\mathbf{x}\mathbf{x}'} = (\mathcal{F}^{-1}(\hat{\mathbf{x}}^* \odot \hat{\mathbf{x}}') + a)^b. \quad (26)$$

Then, computing the kernel correlation for these particular kernels can be done using only a few DFT/IDFT and element-wise operations, in $\mathcal{O}(n \log n)$ time. 

6.2 Radial Basis Function and Gaussian Kernels

RBF kernels have the form $\kappa(\mathbf{x}, \mathbf{x}') = h(\|\mathbf{x} - \mathbf{x}'\|^2)$, for some function h . The elements of $\mathbf{k}^{\mathbf{x}\mathbf{x}'}$ are

$$k_i^{\mathbf{x}\mathbf{x}'} = \kappa(\mathbf{x}', P^{i-1} \mathbf{x}) = h(\|\mathbf{x}' - P^{i-1} \mathbf{x}\|^2). \quad (27)$$

We will show (Eq. (29)) that this is actually a special case of a dot-product kernel. We only have to expand the norm,

$$k_i^{\mathbf{x}\mathbf{x}'} = h(\|\mathbf{x}\|^2 + \|\mathbf{x}'\|^2 - 2\mathbf{x}'^T P^{i-1} \mathbf{x}). \quad (28)$$

The permutation P^{i-1} does not affect the norm of \mathbf{x} due to Parseval's Theorem [21]. Since $\|\mathbf{x}\|^2$ and $\|\mathbf{x}'\|^2$ are constant w.r.t. i , Eq. (28) has the same form as a dot-product kernel (Eq. (23)). Leveraging the result from the previous section,

$$\mathbf{k}^{\mathbf{x}\mathbf{x}'} = h(\|\mathbf{x}\|^2 + \|\mathbf{x}'\|^2 - 2\mathcal{F}^{-1}(\hat{\mathbf{x}}^* \odot \hat{\mathbf{x}}')). \quad (29)$$

As a particularly useful special case, for a Gaussian kernel $\kappa(\mathbf{x}, \mathbf{x}') = \exp(-\frac{1}{\sigma^2} \|\mathbf{x} - \mathbf{x}'\|^2)$ we get

$$\mathbf{k}^{\mathbf{x}\mathbf{x}'} = \exp\left(-\frac{1}{\sigma^2}(\|\mathbf{x}\|^2 + \|\mathbf{x}'\|^2 - 2\mathcal{F}^{-1}(\hat{\mathbf{x}}^* \odot \hat{\mathbf{x}}'))\right). \quad (30)$$

As before, we can compute the full kernel correlation in only $\mathcal{O}(n \log n)$ time. 

6.3 Other Kernels

The approach from the preceding two sections depends on the kernel value being unchanged by unitary transformations, such as the DFT. This does not hold in general for other kernels, e.g. intersection kernel. We can still use the fast training and detection results (Sections 5.2 and 5.3), but kernel correlation must be evaluated by a more expensive sliding window method. 

7 MULTIPLE CHANNELS

In this section, we will see that working in the dual has the advantage of allowing multiple channels (such as the orientation bins of a HOG descriptor [20]) by simply summing over them in the Fourier domain. This characteristic extends to the linear case, simplifying the recently-proposed multi-channel correlation filters [31], [32], [33] considerably, under specific conditions. 

7.1 General Case

To deal with multiple channels, in this section we will assume that a vector \mathbf{x} concatenates the individual vectors for C channels (e.g. 31 gradient orientation bins for a HOG variant [20]), as $\mathbf{x} = [\mathbf{x}_1, \dots, \mathbf{x}_C]$. 

Notice that all kernels studied in Section 6 are based on either dot-products or norms of the arguments. A dot-product can be computed by simply summing the individual dot-products for each channel. By linearity of the DFT, this allows us to sum the result for each channel in the Fourier domain. As a concrete example, we can apply this reasoning to the Gaussian kernel, obtaining the multi-channel analogue of Eq. (30), 

$$\mathbf{k}^{\mathbf{x}\mathbf{x}'} = \exp\left(-\frac{1}{\sigma^2}\left(\|\mathbf{x}\|^2 + \|\mathbf{x}'\|^2 - 2\mathcal{F}^{-1}\left(\sum_c \hat{\mathbf{x}}_c^* \odot \hat{\mathbf{x}}_c\right)\right)\right). \quad (31)$$

It is worth emphasizing that the integration of multiple channels does not result in a more difficult inference problem—we merely have to sum over the channels when computing kernel correlation. 

7.2 Linear Kernel

For a linear kernel $\kappa(\mathbf{x}, \mathbf{x}') = \mathbf{x}^T \mathbf{x}'$, the multi-channel extension from the previous section simply yields

$$\mathbf{k}^{\mathbf{x}\mathbf{x}'} = \mathcal{F}^{-1}\left(\sum_c \hat{\mathbf{x}}_c^* \odot \hat{\mathbf{x}}_c'\right). \quad (32)$$

We named it the Dual Correlation Filter (DCF). This filter is linear, but trained in the dual space α . We will discuss the advantages over other multi-channel filters shortly. 

A recent extension of linear correlation filters to multiple channels was discovered independently by three groups [31], [32], [33]. They allow much faster training times than unstructured algorithms, by decomposing the problem into one linear system for each DFT frequency, in the case of ridge regression. Henriques et al. [31] additionally generalize the decomposition to other training algorithms. 

However, Eq. (32) suggests that, by working in the dual with a linear kernel, we can train a linear classifier with multiple channels, but using only element-wise operations. This may be unexpected at first, since those works require more expensive matrix inversions [31], [32], [33]. 

We resolve this discrepancy by pointing out that this is only possible because we only consider a single base sample \mathbf{x} . In this case, the kernel matrix $K = \mathbf{X} \mathbf{X}^T$ is $n \times n$, regardless of the number of features or channels. It relates the n cyclic shifts of the base sample, and can be diagonalized by the n basis of the DFT. Since K is fully diagonal we can use solely element-wise operations. However, if we consider two base samples, K becomes $2n \times 2n$ and the n DFT basis are no longer enough to fully diagonalize it. This incomplete diagonalization (block-diagonalization) requires more expensive operations to deal with, which were proposed in those works. 

With an interestingly symmetric argument, training with multiple base samples and a single channel can be done in the primal with only element-wise operations

(Appendix A.6). This follows by applying the same reasoning to the non-centered covariance matrix $X^T X$, instead of XX^T . In this case we obtain the original MOSSE filter [9]. 

In conclusion, for fast element-wise operations we can choose multiple channels (in the dual, obtaining the DCF) or multiple base samples (in the primal, obtaining the MOSSE), but not both at the same time. This has an important impact on time-critical applications, such as tracking. The general case [31] is much more expensive and suitable mostly for offline training applications. 

8 EXPERIMENTS

8.1 Tracking Pipeline

We implemented in Matlab two simple trackers based on the proposed KCF, using a Gaussian kernel, and DCF, using a linear kernel. We do not report results for a polynomial kernel as they are virtually identical to those for the Gaussian kernel, and require more parameters. We tested two further variants: one that works directly on the raw pixel values, and another that works on HOG descriptors with a cell size of four pixels, in particular Felzenszwalb's variant [20], [22]. Note that our linear DCF is equivalent to MOSSE [9] in the limiting case of a single channel (raw pixels), but it has the advantage of also supporting multiple channels (e.g. HOG). Our tracker requires few parameters, and we report the values that we used, fixed for all videos, in Table 2. 

The bulk of the functionality of the KCF is presented as Matlab code in Algorithm 1. Unlike the earlier version of this work [29], it is prepared to deal with multiple channels, as the third dimension of the input arrays. It implements three functions: `train` (Eq. (17)), `detect` (Eq. (22)), and `kernel_correlation` (Eq. (31)), which is used by the first two functions. 

The pipeline for the tracker is intentionally simple, and does not include any heuristics for failure detection or motion modeling. In the first frame, we train a model with the image patch at the initial position of the target. This patch is larger than the target, to provide some context. For each new frame, we detect over the patch at the previous position, and the target position is updated to the one that yielded the maximum value. Finally, we train a new model at the new position, and linearly interpolate the obtained values of α and x with the ones from the previous frame, to provide the tracker with some memory. 

8.2 Evaluation

We put our tracker to the test by using a recent benchmark that includes 50 video sequences [11] (see Fig. 1). This dataset collects many videos used in previous works, so we avoid the danger of overfitting to a small subset. 

For the performance criteria, we did not choose average location error or other measures that are averaged over frames, since they impose an arbitrary penalty on lost trackers that depends on chance factors (i.e., the position where the track was lost), making them not comparable. A similar alternative is bounding box overlap, which has the disadvantage of heavily penalizing trackers that do not track across scale, even if the target position is otherwise tracked perfectly. 

Algorithm 1: Matlab code, with a Gaussian kernel.

Multiple channels (third dimension of image patches) are supported. It is possible to further reduce the number of FFT calls. Implementation with GUI available at:
<http://www.isr.uc.pt/~henriques/>

Inputs

- x : training image patch, $m \times n \times c$
- y : regression target, Gaussian-shaped, $m \times n$
- z : test image patch, $m \times n \times c$

Output

- **responses**: detection score for each location, $m \times n$

```
function alphaf = train (x, y, sigma, lambda)
    k = kernel_correlation(x, x, sigma);
    alphaf = fft2(y) ./ (fft2(k) + lambda);
end

function responses = detect (alphaf, x, z, sigma)
    k = kernel_correlation(z, x, sigma);
    responses = real(ifft2(alphaf .* fft2(k)));
end

function k = kernel_correlation (x1, x2, sigma)
    c = ifft2(sum(conj(fft2(x1)) .* fft2(x2), 3));
    d = x1(:)' * x1(:) + x2(:)' * x2(:) - 2 * c;
    k = exp(-1 / sigma^2 * abs(d) / numel(d));
end
```

An increasingly popular alternative, which we chose for our evaluation, is the precision curve [5], [11], [29]. A frame may be considered correctly tracked if the predicted target center is within a distance threshold of ground truth. Precision curves simply show the percentage of correctly tracked frames for a range of distance thresholds. Notice that by plotting the precision for all thresholds, no parameters are required. This makes the curves unambiguous and easy to interpret. A higher precision at low thresholds means the tracker is more accurate, while a lost target will prevent it from achieving perfect precision for a very large threshold range. When a representative precision score is needed, the chosen threshold is 20 pixels, as done in previous works [5], [11], [29]. 

8.3 Experiments on the Full Dataset

We start by summarizing the results over all videos in Table 1 and Fig. 4. For comparison, we also report results for several other systems [3], [4], [5], [7], [9], [14], including some of the most resilient trackers available—namely, Struck and TLD. Unlike our simplistic implementation (Algorithm 1), these trackers contain numerous engineering improvements. Struck operates on many different kinds of features and a growing pool of support vectors. TLD is specifically geared towards re-detection, using a set of structural rules with many parameters. 

Despite this asymmetry, our KCF can already reach competitive performance by operating on raw pixels alone, as can be seen in Fig. 4. In this setting, the rich implicit features induced by the Gaussian kernel yield a distinct advantage over the proposed DCF. 

TABLE 1
Summary of Experimental Results on the 50 Videos Dataset

	Algorithm	Feature	Mean precision (20 px)	Mean FPS
Proposed	KCF	HOG	73.2%	172
	DCF	HOG	72.8%	292
	KCF	Raw	56.0%	154
	DCF	pixels	45.1%	278
Other algorithms	Struck [7]		65.6%	20
	TLD [4]		60.8%	28
	MOSSE [9]		43.1%	615
	MIL [5]		47.5%	38
	ORIA [14]		45.7%	9
	CT [3]		40.6%	64

The reported quantities are averaged over all videos. Reported speeds include feature computation (e.g. HOG).

We remark that the DCF with single-channel features (raw pixels) is theoretically equivalent to a MOSSE filter [9]. For a direct comparison, we include the results for the authors' MOSSE tracker [9] in Fig. 4. The performance of both is very close, showing that any particular differences in their implementations do not seem to matter much. However, the kernelized algorithm we propose (KCF) does yield a noticeable increase in performance.

Replacing pixels with HOG features allows the KCF and DCF to surpass even TLD and Struck, by a relatively large margin (Fig. 4). This suggests that the most crucial factor for high performance, compared to other trackers that use similar features, is the efficient incorporation of thousands of negative samples from the target's environment, which they do with very little overhead.

Timing. As mentioned earlier, the overall complexity of our closed-form solutions is $\mathcal{O}(n \log n)$, resulting in its high speed (Table 1). The speed of the tracker is directly related to the size of the tracked region. This is an important factor when comparing trackers based on correlation filters. MOSSE [9] tracks a region that has the same support as the target object, while our implementation tracks a region that is 2.5 times larger (116×170 on average). Reducing the tracked region would allow us to approach their FPS of 615 (Table 1), but we found that it hurts performance, especially for the kernel variants. Another interesting observation from Table 1 is that operating on 31 HOG features per spatial cell can be slightly faster than operating on raw pixels, even though we take the overhead of computing HOG features into account. Since each 4×4 pixels cell is represented

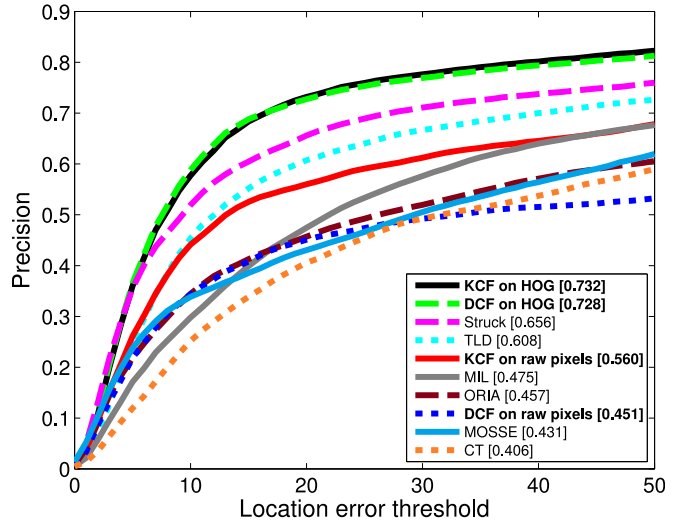


Fig. 4. Precision plot for all 50 sequences. The proposed trackers (bold) outperform state-of-the-art systems, such as TLD and Struck, which are more complicated to implement and much slower (see Table 1). Best viewed in color.

by a single HOG descriptor, the smaller-sized DFTs counterbalance the cost of iterating over feature channels. Taking advantage of all four cores of a desktop computer, KCF/DCF take less than 2 minutes to process all 50 videos ($\sim 29,000$ frames).

8.4 Experiments with Sequence Attributes

The videos in the benchmark dataset [11] are annotated with attributes, which describe the challenges that a tracker will face in each sequence—e.g., illumination changes or occlusions. These attributes are useful for diagnosing and characterizing the behavior of trackers in such a large dataset, without having to analyze each individual video. We report results for four attributes in Fig. 5: non-rigid deformations, occlusions, out-of-view target, and background clutter.

The robustness of the HOG variants of our tracker regarding non-rigid deformations and occlusions is not surprising, since these features are known to be highly discriminative [20]. However, the KCF on raw pixels alone still fares almost as well as Struck and TLD, with the kernel making up for the features' shortcomings.

One challenge for the system we implemented is an out-of-view target, due to the lack of a failure recovery mechanism. TLD performs better than most other trackers in this case, which illustrates its focus on re-detection and failure recovery. Such engineering improvements could probably benefit our trackers, but the fact that KCF/DCF can still outperform TLD shows that they are not a decisive factor.

Background clutter severely affects almost all trackers, except for the proposed ones, and to a lesser degree, Struck. For our tracker variants, this is explained by the implicit inclusion of thousands of negative samples around the tracked object. Since in this case even the raw pixel variants of our tracker have a performance very close to optimal, while TLD, CT, ORIA and MIL show degraded performance, we conjecture that this is caused by their undersampling of negatives.

TABLE 2
Parameters Used in All Experiments

KCF/DCF parameters	With raw pixels	With HOG
Feature bandwidth σ	0.2	0.5
Adaptation rate	0.075	0.02
Spatial bandwidth s	$\sqrt{mn}/10$	
Regularization λ	10^{-4}	

In this table, n and m refer to the width and height of the target, measured in pixels or HOG cells.

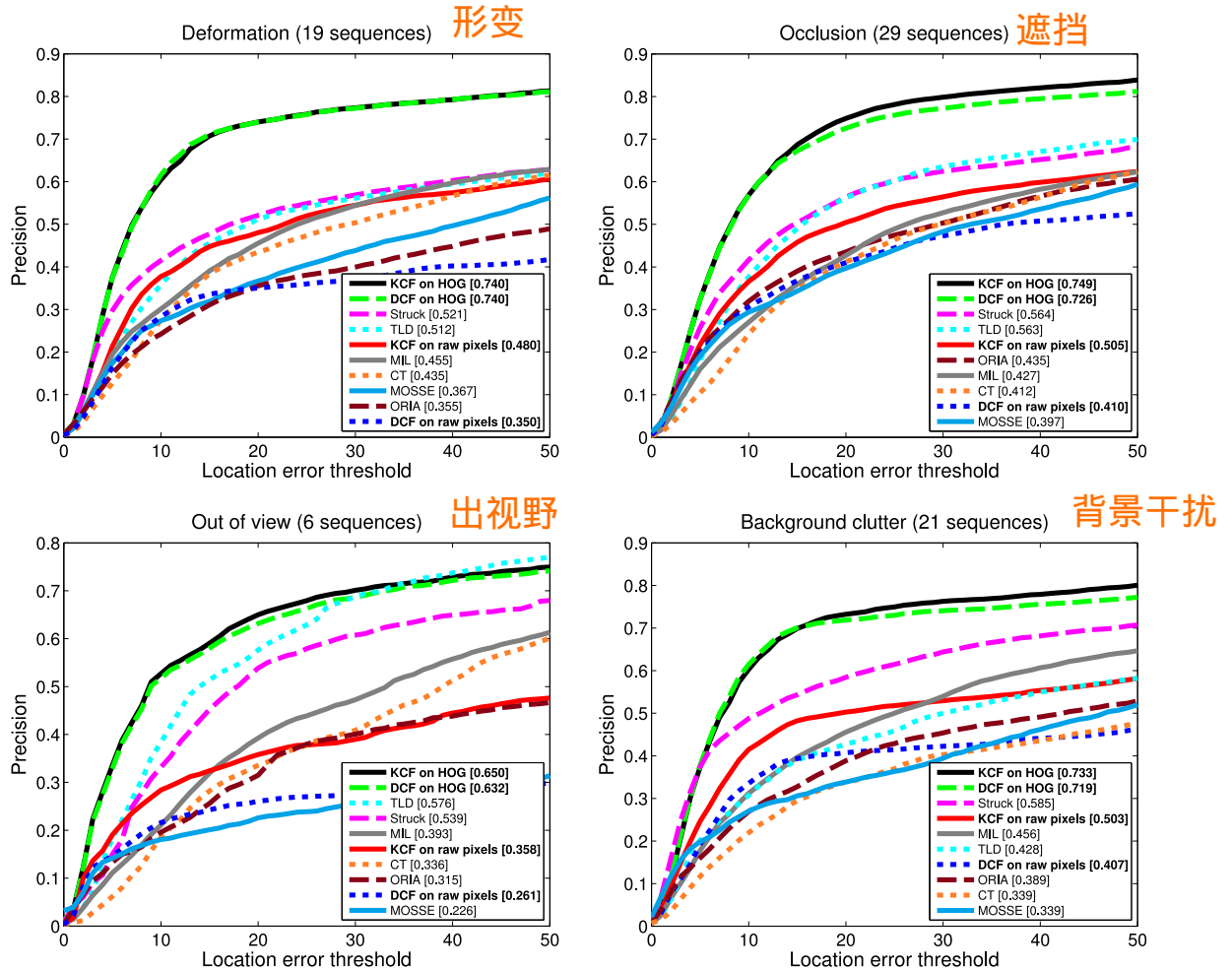


Fig. 5. Precision plot for sequences with attributes: occlusion, non-rigid deformation, out-of-view target, and background clutter. The HOG variants of the proposed trackers (bold) are the most resilient to all of these nuisances. Best viewed in color.

We also report results for other attributes in Fig. 7. Generally, the proposed trackers are the most robust to six of the seven challenges, except for low resolution, which affects equally all trackers but Struck.



9 CONCLUSIONS AND FUTURE WORK

In this study, we demonstrated that it is possible to analytically model natural image translations, showing that under some conditions the resulting data and kernel matrices become circulant. Their diagonalization by the DFT provides a general blueprint for creating fast algorithms that deal with translations. We have applied this blueprint to linear and kernel ridge regression, obtaining state-of-the-art trackers that run at hundreds of FPS and can be implemented with only a few lines of code. Extensions of our basic approach seem likely to be useful in other problems. Since the first version of this work, circulant data has been exploited successfully for other algorithms in detection [31] and video event retrieval [30]. An interesting direction for further work is to relax the assumption of periodic boundaries, which may improve performance. Many useful algorithms may also be obtained from the study of other objective functions with circulant data, including classical filters such as SDF or MACE [25], [26], and more robust loss functions than the

squared loss. We also hope to generalize this framework to other operators, such as affine transformations or non-rigid deformations.



APPENDIX

A.1 Implementation Details

As is standard with correlation filters, the input patches (either raw pixels or extracted feature channels) are

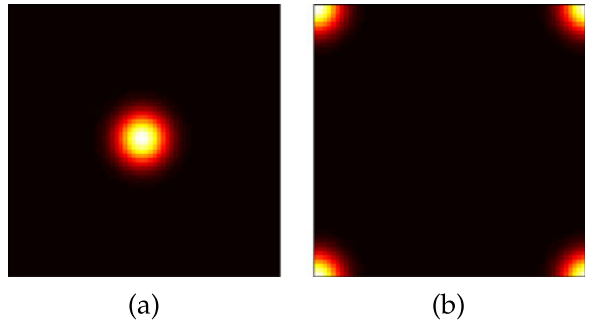


Fig. 6. Regression targets y , following a Gaussian function with spatial bandwidth s (white indicates a value of 1, black a value of 0). (a) Placing the peak in the middle will unnecessarily cause the detection output to be shifted by half a window (discussed in Appendix A.1). (b) Placing the peak at the top-left element (and wrapping around) correctly centers the detection output.



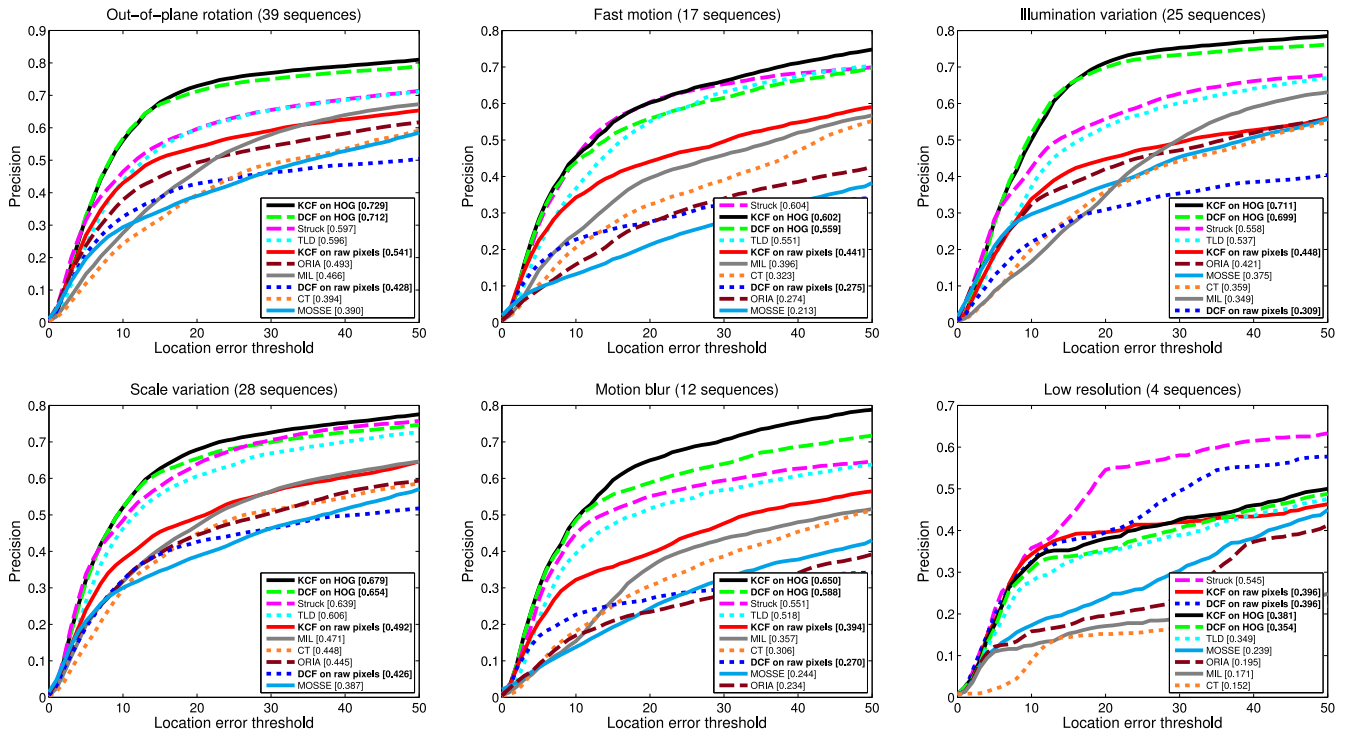


Fig. 7. Precision plots for six attributes of the dataset. Best viewed in color. In-plane rotation was left out due to space constraints. Its results are virtually identical to those for out-of-plane rotation (above), since they share almost the same set of sequences.

weighted by a cosine window, which smoothly removes discontinuities at the image boundaries caused by the cyclic assumption [9], [21]. The tracked region has 2.5 times the size of the target, to provide some context and additional negative samples.

Recall that the training samples consist of shifts of a base sample, so we must specify a regression target for each one in \mathbf{y} . The regression targets \mathbf{y} simply follow a Gaussian function, which takes a value of 1 for a centered target, and smoothly decays to 0 for any other shifts, according to the spatial bandwidth s . Gaussian targets are smoother than binary labels, and have the benefit of reducing ringing artifacts in the Fourier domain [21].

A subtle issue is determining which element of \mathbf{y} is the regression target for the centered sample, on which we will center the Gaussian function. Although intuitively it may seem to be the middle of the output plane (Fig. 6a), it turns out that the correct choice is the top-left element (Fig. 6b). The explanation is that, after computing a cross-correlation between two images in the Fourier domain and converting back to the spatial domain, it is the top-left element of the result that corresponds to a shift of zero [21]. Of course, since we always deal with cyclic signals, the peak of the Gaussian function must wrap around from the top-left corner to the other corners, as can be seen in Fig. 6b. Placing the Gaussian peak in the middle of the regression target is common in some filter implementations, and leads the correlation output to be unnecessarily shifted by half a window, which must be corrected post-hoc.²

2. This is usually done by switching the quadrants of the output, e.g. with the Matlab built-in function `fftshift`. It has the same effect as shifting Fig. 6b to look like Fig. 6a.

Another common source of error is the fact that most implementations of the Fast Fourier Transform³ do not compute the unitary DFT. This means that the L2 norm of the signals is not preserved, unless the output is corrected by a constant factor. With some abuse of notation, we can say that the unitary DFT may be computed as

$$\mathcal{F}_U(\mathbf{x}) = \text{fft2}(\mathbf{x}) / \sqrt{m * n}, \quad (33)$$

where the input \mathbf{x} has size $m \times n$, and similarly for the inverse DFT,

$$\mathcal{F}_U^{-1}(\mathbf{x}) = \text{ifft2}(\mathbf{x}) * \sqrt{m * n}. \quad (34)$$



A.2 Proof of Theorem 1

Under the theorem's assumption that $\kappa(\mathbf{x}, \mathbf{x}') = \kappa(M\mathbf{x}, M\mathbf{x}')$, for any permutation matrix M , then

$$K_{ij} = \kappa(P^i \mathbf{x}, P^j \mathbf{x}) \quad (35)$$

$$= \kappa(P^{-i} P^i \mathbf{x}, P^{-i} P^j \mathbf{x}). \quad (36)$$

Using known properties of permutation matrices, this reduces to

$$K_{ij} = \kappa(\mathbf{x}, P^{j-i} \mathbf{x}). \quad (37)$$

3. For example Matlab, NumPy, Octave and the FFTW library.

By the cyclic nature of P , it repeats every n th power, i.e. $P^n = P^0$. As such, Eq. (37) is equivalent to

$$K_{ij} = \kappa(\mathbf{x}, P^{(j-i)\bmod n} \mathbf{x}), \quad (38)$$

where mod is the modulus operation (remainder of division by n).

We now use the fact the elements of a circulant matrix $X = C(\mathbf{x})$ (Eq. (6)) satisfy

$$X_{ij} = x_{((j-i)\bmod n)+1}, \quad (39)$$

that is, a matrix is circulant if its elements only depend on $(j - i) \bmod n$. It is easy to check that this condition is satisfied by Eq. (6), and in fact it is often used as the definition of a circulant matrix [34].

Because K_{ij} also depends on $(j - i) \bmod n$, we must conclude that K is circulant as well, finishing our proof.

A.3 Kernel Ridge Regression with Circulant Data

This section shows a more detailed derivation of Eq. (17). We start by replacing $K = C(\mathbf{k}^{\mathbf{xx}})$ in the formula for kernel ridge regression, Eq. (16), and diagonalizing it

$$\boldsymbol{\alpha} = (C(\mathbf{k}^{\mathbf{xx}}) + \lambda I)^{-1} \mathbf{y} \quad (40)$$

$$= (F \text{diag}(\hat{\mathbf{k}}^{\mathbf{xx}}) F^H + \lambda I)^{-1} \mathbf{y}. \quad (41)$$

By simple linear algebra, and the unitarity of F ($FF^H = I$),

$$\boldsymbol{\alpha} = (F \text{diag}(\hat{\mathbf{k}}^{\mathbf{xx}}) F^H + \lambda F I F^H)^{-1} \mathbf{y} \quad (42)$$

$$= F \text{diag}(\hat{\mathbf{k}}^{\mathbf{xx}} + \lambda) F^H \mathbf{y}, \quad (43)$$

which is equivalent to

$$F^H \boldsymbol{\alpha} = \text{diag}(\hat{\mathbf{k}}^{\mathbf{xx}} + \lambda)^{-1} F^H \mathbf{y}. \quad (44)$$

Since for any vector $F\mathbf{z} = \hat{\mathbf{z}}$, we have

$$\hat{\boldsymbol{\alpha}}^* = \text{diag}\left(\frac{1}{\hat{\mathbf{k}}^{\mathbf{xx}} + \lambda}\right) \hat{\mathbf{y}}^*. \quad (45)$$

Finally, because the product of a diagonal matrix and a vector is simply their element-wise product,

$$\hat{\boldsymbol{\alpha}}^* = \frac{\hat{\mathbf{y}}^*}{\hat{\mathbf{k}}^{\mathbf{xx}} + \lambda}. \quad (46)$$

A.4 Derivation of Fast Detection Formula

To diagonalize Eq. (21), we use the same properties as in the previous section. We have

$$\mathbf{f}(\mathbf{z}) = (C(\mathbf{k}^{\mathbf{xz}}))^T \boldsymbol{\alpha} \quad (47)$$

$$= (F \text{diag}(\hat{\mathbf{k}}^{\mathbf{xz}}) F^H)^T \boldsymbol{\alpha} \quad (48)$$

$$= F^H \text{diag}(\hat{\mathbf{k}}^{\mathbf{xz}}) F \boldsymbol{\alpha}, \quad (49)$$

which is equivalent to

$$F \mathbf{f}(\mathbf{z}) = \text{diag}(\hat{\mathbf{k}}^{\mathbf{xz}}) F \boldsymbol{\alpha}. \quad (50)$$

Replicating the same final steps from the previous section,⁴

$$\hat{\mathbf{f}}(\mathbf{z}) = \hat{\mathbf{k}}^{\mathbf{xz}} \odot \hat{\boldsymbol{\alpha}}. \quad (51)$$

A.5 Linear Ridge Regression with Circulant Data

This is a more detailed version of the steps from Section 4.4. It is very similar to the kernel case. We begin by replacing Eq. (10) in the formula for ridge regression (Eq. (3)).

$$\mathbf{w} = (F \text{diag}(\hat{\mathbf{x}}^* \odot \hat{\mathbf{x}}) F^H + \lambda I)^{-1} X^H \mathbf{y}. \quad (52)$$

By simple algebra, and the unitarity of F , we have

$$\mathbf{w} = (F \text{diag}(\hat{\mathbf{x}}^* \odot \hat{\mathbf{x}}) F^H + \lambda F I F^H)^{-1} X^H \mathbf{y} \quad (53)$$

$$= (F \text{diag}(\hat{\mathbf{x}}^* \odot \hat{\mathbf{x}} + \lambda)^{-1} F^H) X^H \mathbf{y} \quad (54)$$

$$= F \text{diag}(\hat{\mathbf{x}}^* \odot \hat{\mathbf{x}} + \lambda)^{-1} F^H F \text{diag}(\hat{\mathbf{x}}) F^H \mathbf{y} \quad (55)$$

$$= F \text{diag}\left(\frac{\hat{\mathbf{x}}}{\hat{\mathbf{x}}^* \odot \hat{\mathbf{x}} + \lambda}\right) F^H \mathbf{y}. \quad (56)$$

Then, this is equivalent to

$$F \mathbf{w} = \text{diag}\left(\frac{\hat{\mathbf{x}}^*}{\hat{\mathbf{x}}^* \odot \hat{\mathbf{x}} + \lambda}\right) F \mathbf{y}, \quad (57)$$

and since for any vector $F\mathbf{z} = \hat{\mathbf{z}}$,

$$\hat{\mathbf{w}} = \text{diag}\left(\frac{\hat{\mathbf{x}}^*}{\hat{\mathbf{x}}^* \odot \hat{\mathbf{x}} + \lambda}\right) \hat{\mathbf{y}}. \quad (58)$$

We may go one step further, since the product of a diagonal matrix and a vector is just their element-wise product.

$$\hat{\mathbf{w}} = \frac{\hat{\mathbf{x}}^* \odot \hat{\mathbf{y}}}{\hat{\mathbf{x}}^* \odot \hat{\mathbf{x}} + \lambda}. \quad (59)$$

A.6 MOSSE Filter

The only difference between Eq. (12) and the MOSSE filter [9] is that the latter minimizes the error over (cyclic shifts of) multiple base samples \mathbf{x}_i , while Eq. (12) is defined for a single base sample \mathbf{x} . This was done for clarity of presentation, and the general case is easily derived. Note also that MOSSE does not support multiple channels, which we do through our dual formulation.

⁴ We have $F = F^T$, and $F^* = F^H = F^{-1}$ (unitarity). Note that $F \neq F^H$.

The cyclic shifts of each base sample \mathbf{x}_i can be expressed in a circulant matrix X_i . Then, replacing the data matrix

$$X' = \begin{bmatrix} X_1 \\ X_2 \\ \vdots \end{bmatrix} \text{ in Eq. (3) results in } \quad \boxed{\text{=}}$$

$$\mathbf{w} = \sum_j \left(\sum_i X_i^H X_i + \lambda I \right)^{-1} X_j^H \mathbf{y}, \quad (60)$$

by direct application of the rule for products of block matrices. Factoring the bracketed expression, $\boxed{=}$

$$\mathbf{w} = \left(\sum_i X_i^H X_i + \lambda I \right)^{-1} \left(\sum_i X_i^H \right) \mathbf{y}. \quad (61)$$

Eq. (61) looks exactly like Eq. (3), except for the sums. It is then trivial to follow the same steps as in Section 4.4 to diagonalize it, and obtain the filter equation $\boxed{=}$

$$\hat{\mathbf{w}} = \frac{\sum_i \hat{\mathbf{x}}_i^* \odot \hat{\mathbf{y}}}{\sum_i \hat{\mathbf{x}}_i^* \odot \hat{\mathbf{x}}_i + \lambda}. \quad (62)$$

ACKNOWLEDGMENTS

The authors acknowledge support by the FCT project PTDC/EEA-CRO/122812/2010, grants SFRH/BD75459/2010, SFRH/BD74152/2010, and SFRH/BPD/90200/2012.

REFERENCES

- [1] A. Smeulders, D. Chu, R. Cucchiara, S. Calderara, A. Dehghan, and M. Shah, "Visual tracking: An experimental survey," *IEEE Trans. Pattern Anal. Mach. Intell.*, vol. 36, no. 7, pp. 1442–1468, Jul. 2014.
- [2] H. Yang, L. Shao, F. Zheng, L. Wang, and Z. Song, "Recent advances and trends in visual tracking: A review," *Neurocomput.*, vol. 74, no. 18, pp. 3823–3831, Nov. 2011.
- [3] K. Zhang, L. Zhang, and M.-H. Yang, "Real-time compressive tracking," in *Proc. Eur. Conf. Comput. Vis.*, 2012, pp. 864–877.
- [4] Z. Kalal, K. Mikolajczyk, and J. Matas, "Tracking-learning-detection," *IEEE Trans. Pattern Anal. Mach. Intell.*, vol. 34, no. 7, pp. 1409–1422, Jul. 2012.
- [5] B. Babenko, M. Yang, and S. Belongie, "Robust object tracking with online multiple instance learning," *IEEE Trans. Pattern Anal. Mach. Intell.*, vol. 33, no. 8, pp. 1619–1632, Aug. 2011.
- [6] A. Saffari, C. Leistner, J. Santner, M. Godec, and H. Bischof, "Online random forests," in *Proc. 3rd IEEE Int. Conf. Comput. Vis. Workshop On-line Comput. Vis.*, 2009, pp. 1393–1400.
- [7] S. Hare, A. Saffari, and P. Torr, "Struck: Structured output tracking with kernels," in *Proc. Int. Conf. Comput. Vis.*, 2011, pp. 263–270.
- [8] R. Rifkin, G. Yeo, and T. Poggio, "Regularized least-squares classification," *Nato Sci. Ser. Sub Ser. III*, vol. 190, pp. 131–154, 2003.
- [9] D. S. Bolme, J. R. Beveridge, B. A. Draper, and Y. M. Lui, "Visual object tracking using adaptive correlation filters," in *Proc. Comput. Vis. Pattern Recognit.*, 2010, pp. 2544–2550.
- [10] D. S. Bolme, B. A. Draper, and J. R. Beveridge, "Average of synthetic exact filters," in *Proc. Comput. Vis. Pattern Recognit.*, 2009, pp. 2105–2112.
- [11] Y. Wu, J. Lim, and M. H. Yang, "Online object tracking: A benchmark," in *Proc. Comput. Vis. Pattern Recognit.*, 2013, pp. 2411–2418.
- [12] S. Avidan, "Support vector tracking," *IEEE Trans. Pattern Anal. Mach. Intell.*, vol. 26, no. 8, pp. 1064–1072, Aug. 2004.
- [13] H. Grabner, C. Leistner, and H. Bischof, "Semi-supervised on-line boosting for robust tracking," in *Proc. Eur. Conf. Comput. Vis.*, 2008, pp. 234–247.
- [14] Y. Wu, B. Shen, and H. Ling, "Online robust image alignment via iterative convex optimization," in *Proc. Comput. Vis. Pattern Recognit.*, 2012, pp. 1808–1814.
- [15] L. Sevilla-Lara and E. Learned-Miller, "Distribution fields for tracking," in *Proc. Comput. Vis. Pattern Recognit.*, 2012, pp. 1910–1917.
- [16] C. Lampert, M. Blaschko, and T. Hofmann, "Beyond sliding windows: Object localization by efficient subwindow search," in *Proc. Comput. Vis. Pattern Recognit.*, 2008, pp. 1–8.
- [17] B. Alexe, V. Petrescu, and V. Ferrari, "Exploiting spatial overlap to efficiently compute appearance distances between image windows," in *Proc. Adv. Neural Inf. Processing Syst.*, 2011, pp. 2735–2743.
- [18] H. Harzallah, F. Jurie, and C. Schmid, "Combining efficient object localization and image classification," in *Proc. Int. Conf. Comput. Vis.*, 2009, pp. 237–244.
- [19] A. Vedaldi, V. Gulshan, M. Varma, and A. Zisserman, "Multiple kernels for object detection," in *Proc. Int. Conf. Comput. Vis.*, 2009, pp. 606–613.
- [20] P. Felzenszwalb, R. Girshick, D. McAllester, and D. Ramanan, "Object detection with discriminatively trained part-based models," *IEEE Trans. Pattern Anal. Mach. Intell.*, vol. 32, no. 9, pp. 1627–1645, Sep. 2010.
- [21] R. C. Gonzalez and R. E. Woods, *Digital Image Processing*. Upper Saddle River, NJ, USA: Prentice Hall, 2008.
- [22] P. Dollár, R. Appel, S. Belongie, and P. Perona, "Fast feature pyramids for object detection," *IEEE Trans. Pattern Anal. Mach. Intell.*, vol. 36, no. 8, pp. 1532–1545, Aug. 2014.
- [23] B. Scholkopf and A. Smola, *Learning with Kernels: Support Vector Machines, Regularization, Optimization, and Beyond*. Cambridge, MA, USA: MIT Press, 2002.
- [24] D. Casasent and R. Patnaik, "Analysis of kernel distortion-invariant filters," *Proc. SPIE*, vol. 6764, p. 1, 2007.
- [25] R. Patnaik and D. Casasent, "Fast FFT-based distortion-invariant kernel filters for general object recognition," *Proc. SPIE*, vol. 7252, 2009, p. 1.
- [26] K.-H. Jeong, P. P. Pokharel, J.-W. Xu, S. Han, and J. Principe, "Kernel based synthetic discriminant function for object recognition," in *Proc. IEEE Int. Conf. Acoust. Speech Signal Process.*, 2006, pp. 1–5.
- [27] C. Xie, M. Savvides, and B. Vijaya-Kumar, "Kernel correlation filter based redundant class-dependence feature analysis (KCFA) on FRGC2.0 data," in *Proc. 2nd Int. Conf. Anal. Model. Faces Gestures*, 2005, pp. 32–43.
- [28] A. Mahalanobis, B. Kumar, and D. Casasent, "Minimum average correlation energy filters," *Appl. Optics*, vol. 26, pp. 3633–3640, 1987.
- [29] J. F. Henriques, R. Caseiro, P. Martins, and J. Batista, "Exploiting the circulant structure of tracking-by-detection with kernels," in *Proc. Eur. Conf. Comput. Vis.*, vol. 7575, pp. 702–715, 2012.
- [30] J. Revaud, M. Douze, S. Cordelia, and H. Jégou, "Event retrieval in large video collections with circulant temporal encoding," in *Proc. Comput. Vis. Pattern Recognit.*, 2013, pp. 2459–2466.
- [31] J. F. Henriques, J. Carreira, R. Caseiro, and J. Batista, "Beyond hard negative mining: Efficient detector learning via block-circulant decomposition," in *Proc. Int. Conf. Comput. Vis.*, 2013, pp. 2760–2767.
- [32] H. K. Galoogahi, T. Sim, and S. Lucey, "Multi-channel correlation filters," in *Proc. Int. Conf. Comput. Vis.*, 2013, pp. 3072–3079.
- [33] V. N. Boddeti, T. Kanade, and B. V. Kumar, "Correlation filters for object alignment," in *Proc. Comput. Vis. Pattern Recognit.*, 2013, pp. 2291–2298.
- [34] R. M. Gray, *Toeplitz and Circulant Matrices: A Review*. Boston, MA, USA: Now Publishers, 2006.
- [35] P. J. Davis, *Circulant Matrices*. Providence, RI, USA: Amer. Math. Society, 1994.
- [36] A. Vedaldi and A. Zisserman, "Efficient additive kernels via explicit feature maps," *IEEE Trans. Pattern Anal. Mach. Intell.*, vol. 34, no. 3, pp. 480–492, Mar. 2011.



João F. Henriques received the MSc degree in electrical engineering from the University of Coimbra, Coimbra, Portugal, in 2009. He is currently working toward the PhD degree at the Institute of Systems and Robotics, University of Coimbra. His current research interests include Fourier analysis and machine learning algorithms in general, with computer vision applications in detection and tracking.



Pedro Martins received the MSc and PhD degrees in electrical engineering from the University of Coimbra, Coimbra, Portugal, in 2008 and 2012, respectively. Currently, he is a postdoctoral researcher at the Institute of Systems and Robotics (ISR) in the University of Coimbra. His current research interests include nonrigid image alignment, face tracking, and facial expression recognition.

Rui Caseiro received the BSc degree in electrical engineering (specialization in automation) from the University of Coimbra, Coimbra, Portugal, in 2005. Since 2007, he has been involved in several research projects, which include the European project "Perception on Purpose" and the National project "Brisa-ITraffic." He is currently working toward the PhD degree at the Institute of Systems and Robotics and the Department of Electrical and Computer Engineering, Faculty of Science and Technology, University of Coimbra, where he is also currently a researcher. His current research interests include the interplay of differential geometry with computer vision and pattern recognition.



Jorge Batista received the MSc and PhD degrees in electrical engineering from the University of Coimbra, Coimbra, Portugal, in 1992 and 1999, respectively. He joined the Department of Electrical Engineering and Computers, University of Coimbra, in 1987, as a research assistant where he is currently an associate professor. He was the head of the Department of Electrical Engineering and Computer from the Faculty of Science and Technology of University of Coimbra from November 2011 until November 2013 and is

a founding member of the Institute of Systems and Robotics in Coimbra, where he is a senior researcher. His current research interests include computer vision and pattern analysis related issues, including real-time vision, video surveillance, video analysis, nonrigid modeling and facial analysis. More recently his research activity also focus on the interplay of Differential Geometry in computer vision and pattern recognition problems. He has been involved in several national and European research projects, several of them as PI at UC.

▷ For more information on this or any other computing topic, please visit our Digital Library at www.computer.org/publications/dlib.

KCF的主要贡献:

- 1.使用目标周围区域的循环矩阵采集正负样本，利用脊回归训练目标检测器，并成功的利用循环矩阵在傅里叶空间可对角化的性质将矩阵的运算转化为向量的Hadamard积，即元素的点乘，大大降低了运算量，提高了运算速度，使算法满足实时性要求。
- 2.将线性空间的脊回归通过核函数映射到非线性空间，在非线性空间通过求解一个对偶问题和某些常见的约束，同样的可以使用循环矩阵傅里叶空间对角化简化计算。
- 3.给出了一种将多通道数据融入该算法的途径。

Abstract:

1. 传统跟踪器：使用平移尺度化的 sample patches
2. 本文提出的是：基于数千个平移 patches 的一个分析模型。

结果矩阵是一个循环矩阵

使用离散傅里叶变换对数据结果矩阵对角化

也可以将存储和计算减少几个数量级

3. KCF 线性分类算法有相同复杂度 $O(n \log n)$

Introduction

1. 跟踪任务是一个在线学习问题。

2. 判别分类器的任务：将背景目标分离开

(Patch 只有两个目标：跟踪对象、非跟踪对象(统称为“背景”))

3. 人们一般只关注正样本，但负样本同样重要，甚至更重要。

在一张图中，正样本的数量是有限的，而负样本的数量是无限的。

但是取太多样本又会使计算复杂度增大，因此都是在保证样本数量与低计算间寻找平衡。

4. 在傅里叶域内，可以实现对相对平移后的数千个样本进行分析，而不需要迭代。

使用的工具：循环矩阵。

5. 本文提出的是基于内核的脊回归分类器。

一种特殊的最小二乘。

Related work

1. 为使跟踪更有效，必须有在线学习—更新模型。

2. 多通道，现代特征 (梯度直方图 HOG)

Contributions

1. 在 CSK 中已经提出：脊回归 → 循环移位，傅里叶变换 → 加快速度，循环移位闭环解。

2. KCF 特征：HOG 特征 → 性能优于只使用 Pixel。

4. 线性回归

脊回归，其性能与 SVM 几乎一致，并且有简单的闭环解。

$$\min_{w \in \mathbb{R}^n} (f(x_i) - y_i)^2 + \lambda \|w\|^2 \quad (1)$$

得到闭环解为： $w = (X^T X + \lambda I)^{-1} X^T y$ (2) 这是最小二乘的解

这个推导过程在 Andrew Ng 的 machine learning 课中推导过，笔记中有记录，CSDN 中《机器学习_正规方程(最小二乘法)推导》。

进入到傅里叶领域式(2)变成： $w = (X^H X + \lambda I)^{-1} X^H y$ ，其中 X^H 为 X 的共轭转置。

这样 X^H ：因为由 $F(f \circ g) = F(f)^* \cdot F(g)$ \Rightarrow 所以式(2)在傅里叶域内就变成了式(3)

4.2 循环平移

$$\begin{bmatrix} 0 & 0 & \cdots & 0 & 1 \\ 1 & 0 & \cdots & 0 & 0 \\ 0 & 1 & \cdots & 0 & 0 \\ \vdots & 0 & \cdots & 1 & 0 \end{bmatrix}$$

1. 置换矩阵： $P = \begin{bmatrix} 0 & 0 & \cdots & 0 & 1 \\ 1 & 0 & \cdots & 0 & 0 \\ 0 & 1 & \cdots & 0 & 0 \\ \vdots & 0 & \cdots & 1 & 0 \end{bmatrix}$ ， $P^H X$ ，将 X 循环平移多少次。

2. 由于在进行循环平移时，最后一个元素平移可能会造成图像失真；但这可以通过适当的 Padding 或加窗减轻。

Appendix 1: 1. 使用余弦窗加权，可以平滑的消除由循环假设引起的图像边界的不连续性。

2. 由二维傅里叶本身性质：若 $fft2$ 变换时，变换矩阵原点设在中心，则其频谱能量集中分布在变换系数矩阵的中心附近，若 $fft2$ 变换矩阵原点设在左上角，那么其频谱能量分布四个角上。

而 MATLAB 内置 $fft2$ 变换函数的变换矩阵原点设在左上角，因此导致了在 MATLAB 中对图像进行 $fft2$ 变换后，图像能量集中在四角，与图像标签不对应了，所以要使用 MATLAB 中的 $fftsift2$ 函数将零频分量移到频谱中心。

3. 零频分量，位于低频区域，由 $fft2$ 对图像进行变换后，可以看出图像能量主要集中在低频区域。

4. 说明一点：在 Matlab, Numpy, octave 和 FFTW 等中实现 FFT 时，并不会计算单-DFT (离散傅里叶变换)

单一 DFT 计算式： $F(x) = fft2(x) / \sqrt{m \cdot n}$ ，输入 X 为 $m \times n$ 矩阵。

则单一逆 DFT： $f(x) = ifft2(x) * \sqrt{m \cdot n}$

3. 由于循环的性质：① 循环几次就可以全部采样信息。

② 本文中将前半部分看作是正方向上的移位，后半部分看作是负方向上的移位。

4.3 循环矩阵

注：所有的循环矩阵都能通过傅里叶变换进行对角化，即： $X = C(X) = F \text{diag}(\hat{X}) F^H$

其中， \hat{X} 是向量 X 的傅里叶变换， F 是傅里叶变换矩阵，上标 H 表示转置： $X^H = (X^*)^T$

换句话说， X 相似于对角阵， X 的特征值是 ω 的元素。

→ 反过来说：若一个矩阵能够表示为两个傅里叶矩阵乘以一个对角矩阵的乘积形式，则它是一个循环矩阵。其生成向量是向量元素的傅里叶逆变换，即： $F^H \cdot \text{diag}(Y) \cdot F = C(F^H(Y))$

下面进行具体解释：

① X 是原生向量 x 生成的循环矩阵。以矩阵尺寸 $N=4$ 为例：

$$X = C(X) = \begin{bmatrix} X_1 & X_2 & X_3 & X_4 \\ X_4 & X_1 & X_2 & X_3 \\ X_3 & X_4 & X_1 & X_2 \\ X_2 & X_3 & X_4 & X_1 \end{bmatrix}$$

② F 是离散傅里叶矩阵 (DFT matrix)，可以用一个复数 $w = e^{-j2\pi/Nk}$ 表示，其中 N 为方阵下的尺寸，以 $N=4$ 为例：

$$F = \frac{1}{\sqrt{N}} \begin{bmatrix} 1 & 1 & 1 & 1 \\ 1 & w & w^2 & w^3 \\ 1 & w^2 & w^4 & w^6 \\ 1 & w^3 & w^6 & w^9 \end{bmatrix}$$

把 w 想象成一个角度为 $\frac{2\pi}{N}$ 的向量，这个矩阵的每一行是这个向量在不断旋转。从上到下，旋转速度越来越快。

之所以称为 DFT matrix，是因为一个信号的 DFT 变换可以用此矩阵乘积获得：

$$\hat{x} = DFT(x) = \sqrt{N} F^H x$$

反傅里叶变换也可以通过类似手段得到：

$$x = \frac{1}{\sqrt{N}} F \hat{x}$$

★ 傅里叶矩阵有许多性质：

一是对称矩阵，由上面观察 w 的规律即可知。

一满足 $F^H F = F F^H = I$ ，也就是说真是酉矩阵，可以通过将 F 展成 w 来验证。

注：可以看到 F 为常数，可以提前计算好，占算处理的 x 没关系。

③ 对角化如何理解 y 。

把 $X = C(X) = F \text{diag}(\hat{X}) F^H$ ，两边乘以逆矩阵，得：

$$F^H X \cdot (F^H)^{-1} = \text{diag}(\hat{X})$$

F 为酉矩阵 $\Rightarrow F^H F = I$

对于矩阵 $F^H F = I \Rightarrow F^H = F^{-1}$

则： $F^H X \cdot (F^H)^{-1} = F^H X \cdot F = \text{diag}(\hat{X})$

也就是说：矩阵 X 通过相似变换下变成对角阵 $\text{diag}(\hat{X})$ ，则对循环矩阵 X 进行对角化。

另外， $F^H X F$ 是矩阵 X 的 2D DFT 变换。即傅里叶变换可以把循环矩阵对角化。

④ 证明

证明在 EndNote 的 reference 栏中的《循环矩阵及其对角化》。

$$4.4 X^H X = F \cdot \text{diag}(\hat{X}^*) \cdot F^H \cdot F \cdot \text{diag}(\hat{X}) \cdot F^H$$

因为： $F^H F = I$

所以： $X^H X = F \cdot \text{diag}(\hat{X}^*) \cdot \text{diag}(\hat{X}) \cdot F^H$

因为在对角阵上对元素优化是在元素之间的。

所以： $X^H X = F \cdot \text{diag}(\hat{X}^* \otimes \hat{X}) \cdot F^H$

而 $\hat{X}^* \otimes \hat{X}$ 可以看作是信号 X 的自相关

Appendix 5:

$$Eq.(3): W = (X^H X + \lambda I)^{-1} X^H y$$

而 X 本身就是一个循环矩阵，其生成向量为 $[1, 0, 0, \dots, 0]$ ，这个生成向量的傅里叶变换为全 1 向量 $\delta = [1, 1, 1, \dots, 1]$

$$\begin{aligned} \text{则: } W &= [F \cdot \text{diag}(\hat{x}^* \odot \hat{\delta}) F^H + \lambda F \cdot I F^H]^{-1} X^H y \\ &= [F \cdot \text{diag}(\hat{x}^* \odot \hat{\delta}) F^H + \lambda F \cdot \text{diag}(\delta) F^H]^{-1} X^H y \\ &= [F \cdot \text{diag}(\frac{1}{\hat{x}^* \odot \hat{\delta}}) F^H]^{-1} X^H y. \quad \text{根据循环矩阵求逆性质, 可以把矩阵求逆转} \\ &\quad \text{换成特征值求逆.} \\ &= F \cdot \text{diag}(\frac{1}{\hat{x}^* \odot \hat{\delta}}) F^H F \cdot \text{diag}(\delta) F^H y \quad Eq.(7): X = F \cdot \text{diag}(\hat{x}) \cdot F^H \Rightarrow X^H = F \cdot \text{diag}(\hat{x}^*) \cdot F^H \\ &= F \cdot \text{diag}(\frac{1}{\hat{x}^* \odot \hat{\delta}}) - \text{diag}(\hat{x}^*) \cdot F^H \cdot y \quad \text{论文中这个地方是错的} \\ &= F \cdot \text{diag}(\frac{\hat{x}^*}{\hat{x}^* \odot \hat{\delta} + \lambda}) \cdot F^H \cdot y \quad \text{对角化性质为 Eq.(6): } X = C(X) = F \cdot \text{diag}(\hat{x}) \cdot F^H \quad \text{向量} \quad \text{向量 } \delta \text{ 的傅里叶变换} \\ &= C(F^{-1}(\frac{\hat{x}^*}{\hat{x}^* \odot \hat{\delta} + \lambda})) \cdot y \quad \text{对角化性质: } F \cdot \text{diag}(y) \cdot F^H = C(F(y)) \\ \text{由循环矩阵卷积性质: } F[Cx] \cdot y &= \hat{x}^* \odot \hat{y} \end{aligned}$$

则: $F(w) = (\frac{\hat{x}^*}{\hat{x}^* \odot \hat{\delta} + \lambda})^* \odot F(y)$
由于 $\hat{x}^* \odot \hat{\delta}$ 后其每个元素都变成了实数，因此其共轭不变。

则: $F(w) = \frac{\hat{x}^*}{\hat{x}^* \odot \hat{\delta} + \lambda} \odot F(y)$
 $= \frac{\hat{x}^* \odot \hat{y}}{\hat{x}^* \odot \hat{\delta} + \lambda}$ 论文中这里分子为 $\hat{x}^* \odot \hat{y}$ 是错误的，但代码中没有涉及。

则: $\hat{w} = \frac{\hat{x}^* \odot \hat{y}}{\hat{x}^* \odot \hat{\delta} + \lambda}$

可知，可以使用逆 FFT 很容易恢复为时间域内 w 。

5.1 核技巧回顾

① 将 w 映射到非线性特征空间: $w = \sum \alpha_i \varphi(x_i)$

因此优化的变量是 α ，而不是 w 。

② 点积算法形式: $(\varphi(x) | \varphi(x')) = k(x, x')$

③ 所有样本的点积存储为一个 $n \times n$ 矩阵 K , $K_{ij} = k(x_i, x_j)$

④ 核技巧隐式的使用高维特征空间 U ，没有在该空间中实现冗余量。

这也是一个很大的缺点，因为线性空间的函数复杂度将会随着样本数量而增加。

$$f(z) = w^T z = \sum_i \alpha_i k(z_i, z_i)$$

而在后续介绍中，会展示在假设遵循循环的前提下，最大限度避免缺点。

5.2 快速核回归

① 背归的闭环解为: $\alpha = (K + \lambda I)^{-1} y$.

其中 K 是核矩阵， y 是系数 α 的向量。

② 定理 1：给出循环数据 $C(x)$ ，对于任意置换矩阵 P ，如果核函数满足 $k(x, x') = k(mx, mx')$ ，那么相关核矩阵 K 是循环的。

Appendix 2: 证明定理 1

根据假设，对于任意置换矩阵 P , $k(x, x') = k(mx, mx')$,

$$\text{则: } K_{ij} = k(P^i x, P^j x) = k(P^{-1} P^i x, P^{-1} P^j x) = k(x, P^{j-i} x)$$

由 P 的循环性质知: $P^n = P^0$

$$\text{则: } K_{ij} = k(x, P^{(j-i) \bmod n} x), \quad \text{其中 mod 为取模运算 (除后的余数)}$$

$$Eq.(6) \quad x = Cx = \begin{bmatrix} x_1 & x_2 & x_3 & \cdots & x_n \end{bmatrix} \quad \text{满足 } x_{ij} = x_{(j-i) \bmod n + 1}$$

也就是说若矩阵元素仅取决于 $(j-i)$ ，则矩阵是循环的。这经常作为循环矩阵的定义。

由定理 1 可知 K 是循环的。

因此我们对角化 K 得到: $\alpha = \frac{g}{k^* + \lambda}$ ，其中 \hat{k}^* 为 FFT 向量， K^* 是核矩阵 $K = C(K^*)$ 的第一行。

Appendix 3: 循环数据的核脊回归

附录 3 的推导和上面附录 5 的推导原理是一样的。

$$\alpha = (K + \lambda I)^{-1} y$$

$$= [F \cdot \text{diag}(\hat{K}) F^H + F \cdot \text{diag}(\lambda I) F^H]^{-1} y$$

$$= [F \cdot \text{diag}(\hat{K} + \lambda I) F^H] \cdot y$$

$$= F \cdot \text{diag}(\frac{1}{\hat{K} + \lambda I}) \cdot F^H \cdot y$$

$$= C(F(\frac{1}{k+\lambda\delta})) \cdot y$$

$$\text{由 } F(C(x)y) = x^* \circ \hat{y} \text{ 得, } F(k) = (\frac{1}{k+\lambda\delta})^* \circ \hat{y} \Rightarrow k = (\frac{1}{k+\lambda\delta})^* \circ \hat{y}$$

这里 k 是核相关矩阵第 i 行，表示原始生成向量 x^* 移位 i 的向量 y^* 的核函数，考察其对于对称位置上的两个元素。

$$k_i = k(x^*, x^i), \quad k_{ii} = k(x^*, x^{*i})$$

补充
笔记

我们涉及到的核函数都只和位移绝对值有关，因此对于核 $k(a, b)$ ，有： a 在移 i 位 = b 在移 i 位 = b 在移 $N-i$ 位。

举个例子：定义一个内积形式核函数： $k(a, b) = \text{inner_product}(a, b) = a_0b_0 + a_1b_1 + a_2b_2$

$$a \text{右移 } 1 \text{ 位: } k(a_1, b) = \text{inner_product}(a_1, b) = [a_0, a_1, a_2][b_0, b_1, b_2]^T = a_0b_0 + a_1b_1 + a_2b_2$$

$$b \text{ 左移 } 1 \text{ 位: } k(a, b_1) = \text{inner_product}(a, b_1) = [a_0, a_1, a_2][b_1, b_2, b_3]^T = a_0b_1 + a_1b_2 + a_2b_3$$

$$b \text{ 在移 } (3-i) \text{ 位: } k(a, b_2) = \text{inner_product}(a, b_2) = [a_0, a_1, a_2][b_2, b_3, b_0]^T = a_0b_1 + a_1b_2 + a_2b_3$$

再细致的解释： $k(x_0, x_1)$: x_0 向右移 $2-i$ 位， $k(x_0, x_{N-i})$: x_0 向右移 $N-i$ 位。

因为向量长度为 N ，因此 $k(x_0, x_{N-i})$ 为右向左移 $i-1$ 位，即向左移 i 位。

k 的定义使得结果只和“相对”位移有关，即：右移位 $N-i$ 位 = 左移位 i 位 = 右移 i 位。

由上面补充可知， k 为对称向量，而对称向量的傅里叶变换为实数。

$$\text{则: } k = (\frac{1}{k+\lambda\delta})^* \circ \hat{y} = (\frac{1}{k+\lambda\delta}) \circ \hat{y} = \frac{\hat{y}}{k+\lambda\delta}$$

③ 为了更好地理解 k^x ，本文定义一个更加通用化的内核。两个任意向量 X 和 X' 的核相关是具有元素的向量

$$k_i^x = k(X^i, P^{i+1}X)$$

换句话说，它包含针对两个参数的不同相对位移进行评估的核。

核 k^x 在傅里叶领域是 X 真的核相关，在线性情况下，称之为自相关。

因为点积算法形式： $(Q^i(X) Q(X)) = R(X, X')$

所以： $k_i^{xx} = k(X^i, P^{i+1}X) = Q^i(X) Q(P^{i+1}X)$ ，其中 X 与 X' 在高维空间内是互相关的。

④ 从优化又并不是解决加速的唯一问题，还要考虑检测阶段。

5.3 快速检测

所有待检测样本和所有训练样本的核相关矩阵为 K ，每一列对应一个待测样本。可以一次计算所有样本的响应 ($N \times 1$ 向量)

$$y = k^T \cdot a$$

$$= C(k)^T \cdot a$$

利用循环矩阵转置性质， $C(k)^T$ 特征值为 K ，则 $C(k)^T$ 的特征值为 K^*

$$\text{则: } y' = C(k)^T \cdot a = C(K^*) \cdot a$$

利用循环矩阵卷积性质： $F(C(X)y) = X^* \circ \hat{a}$

$$\text{则: } F(y') = F(C(K^*) \cdot a) = (\hat{K}^*)^* \circ \hat{a} \\ = \hat{K} \circ \hat{a}$$

7. 多通道

在多通道情况下（例如使用了 HOG 特征），生成向量 X 变成 $M \times L$ ，其中 M 是样本像素数， L 是特征维度。在上述所有计算中，需要更改的只有向量的内积：

$$x'y = \sum_i C(X^i)^T y^i$$